DIRECT NUMERICAL SIMULATION OF INTERACTIONS BETWEEN BUBBLES AND WALL-TURBULENCE

Takafumi Kawamura
Ship Performance Division, National Maritime Research Institute
6-38-1 Shinkawa, Mitaka, Tokyo 181-0004, Japan
kawamura@srimot.go.jp

Yoshiaki Kodama
Ship Performance Division, National Maritime Research Institute
6-38-1 Shinkawa, Mitaka, Tokyo 181-0004, Japan
kodama@srimot.go.jp

ABSTRACT

A new computational method for investigating interactions between bubbles and turbulence has been developed. Both liquid and gas phases are treated as incompressible continuum fluids and solved by a finite volume method, while the interface between the phases is resolved by a front-tracking method. The accuracy of the method is validated for the problem of a single rising bubble. The method has been applied to a direct numerical simulation (DNS) of a fully developed turbulent channel flow containing bubbles. The results of DNS computations suggest that large bubbles can be preferable for the frictional drag reduction at low Reynolds numbers.

INTRODUCTION

About 80% of the total propulsion resistance of a ship like a tanker is due to friction with the surrounding water. It will be a great contribution to the environment to reduce the fuel consumption of ships as a means of mass transportation by reducing the frictional drag. There are several devices for reducing the frictional resistance such as passive type devices like riblets or active type devices like the combination of micro sensors and actuators. Among these methods, we consider the microbubble injection method is most suitable for ships.

There is relatively large extent of literature on the microbubble drag reduction. McCormick et al. (1973) found that the drag of a submerged body was reduced by microbubbles produced by electrolysis. Madavan et al. (1985) investigated the relation between the drag reduction and the mean void ratio for a developing turbulent boundary layer on a flat plate. Guin et al. (1996) experimentally showed that the drag reduction is better correlated with the void fraction near the wall than the mean value. Takahashi et al. (1997) investigated the microbubble drag reduction for a fully developed turbulent boundary layer in a channel.

The drag reduction rate for given amount of microbubbles must be improved in order to make the microbubble drag reduction method fit for practical use. For this purpose, it is important to understand the mechanism of the microbubble drag reduction. Although decrease in the mean density, increase in the effective viscosity, and modulation of turbulence are assumed to be responsible, convincing answers are still missing.

For developing an advanced model to explain and predict the microbubble drag reduction, more detailed experimental data is needed. However, since the presence of microbubbles strongly hinders measurements by LDV or PIV, the numerical simulation is expected to be an effective alternative approach. In this study we aim at obtaining a detailed data of the velocity field of turbulent flow modified by microbubbles. The numerical simulation is also useful for investigating the influences of the factors such as bubble size, bubble deformation or buoyancy, since it is very difficult to control these parameters independently in experiments.

Two-phase flow simulation methods are classified into three categories. The first way is to solve phase-averaged equations of fluid motion, and the second way is to model bubbles

by point force distributions. These approaches are valid for predicting macroscopic feature of the flow, or in particular cases when the size of bubbles can be assumed infinitely small. The third way is to simulate the two-phase flow directly with implementing the continuity of mass and momentum across the air-water interface. Altough the computational load is highest, only this method can resolve the full interactions between two phases. Figure 1 shows a snap photo of the flow dealt with in this study. It is noted that the size of bubbles is relatively large, and the effect of the deformation of bubbles is supposed to be significant. Therefore, we adopt a direct numerical simulation method. Kanai and Miyata (1998) carried out a direct numerical simulation of turbulent Couette flow containing bubbles by use of the marker density method. We apply a similar computational method to a fully developed turbulent channel flow containing bubbles.

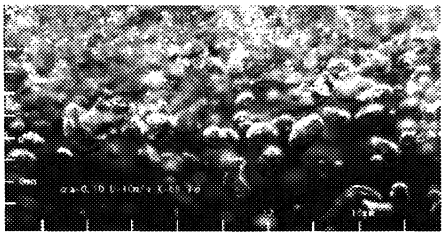

Figure 1: Photograph of bubbles in the channel (Takahashi et al., 1997)

NUMERICAL METHOD

Governing equations

Both water and air phases are treated as incompressible fluids, and the continuity of stress is implemented at the interface. The governing equations for each phase are the Navier-Stokes equation,

$$\frac{\partial u_i}{\partial t} = -\frac{\partial u_i u_j}{\partial x_j} + \frac{\partial}{\partial x_j}\left\{\nu\left(\frac{\partial u_i}{\partial x_j} + \frac{\partial u_j}{\partial x_i}\right)\right\} - \frac{1}{\rho}\frac{\partial p}{\partial x_i} \tag{1}$$

and the continuity equation

$$\frac{\partial u_i}{\partial x_i} = 0 \tag{2}$$

where x_i, u_i, and p are the Cartesian coordinate, the velocity components, and static pressure respectively. The fluid density ρ and the kinematic viscosity ν take values of either water or air depending on whether the center of the computational cell is water or air.

Interface tracking method

There are several methods for expressing the moving interface between two fluids, such as the VOF method (Hirt and Nichols, 1981), the level-set method (Osher and Sethian, 1988), and the front-tracking method (Unverdi and Tryggvason, 1992). The VOF and level-set methods are categorized as the front capturing methods which track the movement of volume and find the interface in an indirect way. One of the merits of the methods of this type is that collision and breakup of interfaces are easily treated. On the other hand, the front-tracking method tracks the interface directly allowing more accurate calculation of the curvature of the interface, although treatment of surface restructuring is complicated. We use the front-tracking method, since accurate calculation of the interface curvature is very important for the case investigated in this study.

Each bubble is expressed by its center position and radius distribution around the center as shown in Figure 2. Marker particles are placed on each bubble regularly on a two-dimensional spherical grid (θ, ϕ). In the beginning of each time step, the positions of the marker particles are updated using the velocity interpolated from the rectangular grid for solving the Navier-Stokes equations. After the marker particles are moved, the position of the center is updated. Then the radius at each point $r(\theta, \phi)$ around the new center is calculated and expanded in a series of spherical harmonic function,

$$r(\theta,\phi) = \sum_{n=0}^{N}\sum_{m=0}^{n} P_{nm}(\cos\theta)\{A_{nm}\cos m\phi + B_{nm}\sin m\phi\} \tag{3}$$

in which N is the number of the deformation modes considered, P_{nm} is Legendre associate polynomial. N is set to 8 in this study. The coefficients A_{nm} and B_{nm} are obtained by numerical integrations.

The primary merit of this merit is that the curvature of the interface is accurately computed with relatively small number of grid points. Another advantage is that deformations of high wave number modes, which give rise to numerical instabilities, can be filtered out. Whereas the shortcomings are that the radius must be a single-valued function of the altitude and latitude. Therefore, this method cannot deal with deformations beyond a certain limit, collision or separation of bubbles.

Solution algorithm

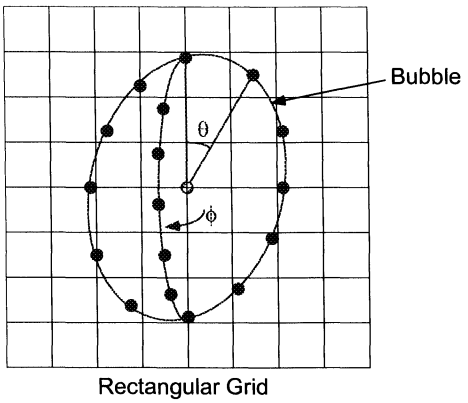

Figure 2: Schematic sketch of the front-tracking method

A second-order finite volume method is used for the spatial discretization on a rectangular grid system fixed to the space, and a second-order semi-implicit fractional step method is used for the time integration. At the beginning of each time step, the positions and shapes of bubbles are determined, and the values of density and the kinematic viscosity in each cell are set to values of water or air. Whether a cell-center point is inside a bubble or not is judged from the expression (3). Then the dynamic boundary condition is set in cells containing interfaces. The surface tension is treated as a pressure jump across the interface. The curvature of the interface is calculated from the expression (3) analytically. Using this interface boundary condition the momentum equations (1) are semi-implicitly integrated, and then corrected by solving a Poisson equation for the pressure. The Poisson equation for the pressure is solved by a multigrid method.

SINGLE RISING BUBBLE

The accuracy of the computational method is examined for the problem of a single bubble rising in quiescent water. Computations are carried out using $64 \times 64 \times 64$ cells for a domain of 4 diameters cube, which moves with the center of the bubble. Figure 3 shows a comparison of the computed drag coefficient C_D and an empirical formula proposed by Tomiyama et al. (1995). Bubbles smaller than 1 mm are almost spherical and rise straight up, while larger bubbles are deformed and show non-axisymmetric swing motions. Computations reproduce this behavior very well, and the calculated values of C_D are in good agreement with the empirical formula. Figure 4 shows computed ellipsoidal shape of the bubble. The flatness is confirmed to be also in good agreement with experiments.

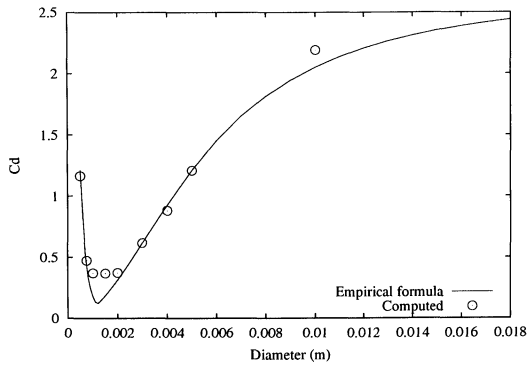

Figure 3: Drag coefficient of a single rising bubble in clean water

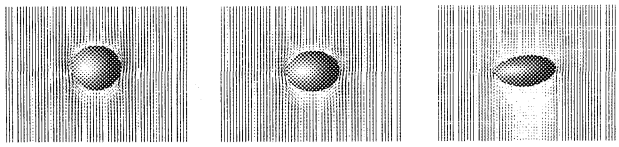

Figure 4: Computation of a single rising bubble in water

DNS OF A TURBULENT CHANNEL FLOW CONTAINING BUBBLES

Condition of computations

A fully developed turbulent channel flow containing bubbles is investigated by the present numerical method. Before introducing the bubbles, a fully developed single-phase turbulent channel flow at the Reynolds number $Re_\tau = 180$, based on the friction velocity u_τ and a half width of the channel H, was computed. The size of the computational domain is set to $6.4H \times 2H \times 3.2H$, in the streamwise, wall-normal and spanwise directions respectively. A periodic boundary condition is used in the streamwise and spanwise directions. The x-, y- and z- axes are taken in the streamwise, wall-normal and spanwise directions respectively. The profiles of computed mean velocity and turbulence intensity agree well with the DNS results of Kim et al. (1986) as shown in Figure 5.

A total of eight DNS runs are performed for investigating the influences of the parameters such as the void ratio, the bubble size, buoyancy, and surface tension on the drag reduction. The parameters are summarized in Table 1. Although the Reynolds number $Re_\tau = 180$ is an order of magnitude smaller, the other parameters are on the same order as in the experiment by Takahashi et al. (1997). When the Reynolds number is small, the increase in the effective viscosity is supposed to dominate over the decrease in the density and the modulation of turbulence. Therefore, the

Run	We	$1/Fr^2$	D^+	N_B	α (%)	C_f
0	-	0	-	-	0.0	1.0
1	9.2	0	90	54	8.6	1.23
2	37.0	0	90	54	8.6	1.16
3	9.2	0	90	18	2.9	1.12
4	37.0	0	90	18	2.9	1.12
5	9.2	6.8×10^3	90	18	2.9	1.11
6	7.3	0	71.4	36	2.9	1.15
7	7.3	5.4×10^3	71.4	36	2.9	1.12
8	11.6	0	113	9	2.9	1.10

Re_τ	Reynolds number	$Re_\tau = u_\tau H/\nu$
We	Weber number	$We = \rho U_m^2 D/\sigma$
σ	Surface tension coefficient	
Fr	Froude number	$Fr = U_m/\sqrt{gD}$
g	Gravitational acceleration	
D	Bubble diameter	
D^+	Bubble diameter in viscous unit	$D^+ = Du_\tau H/\nu$
N_B	Number of bubbles	
α	Mean void ratio	
C_f	Normalized friction coefficient	

Table 1: Condition of computations

frictional drag is also supposed to increase.

Computation with bubbles are initialized with the result of the single-phase flow computation, and bubbles are suddenly introduced as shown in Figure 6 at the non-dimensional time $t^+ = u^2 t/\nu = 0$. The mean pressure gradient is automatically adjusted so that the volume flow rate is kept constant.

Results

Figure 7 shows the time histories of the normalized mean wall shear stress C_f for the DNS runs 0 and 3 and 6. After the bubbles are introduced at $t^+ = 0$, the mean wall shear stress increases and reaches a steady level at $t^+ = 400 \sim 800$. The average values of C_f after reaching the steady level are shown in the Table 1.

Figure 8 shows the values of C_f versus four

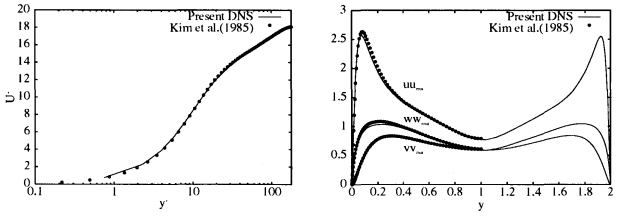

Mean velocity Turbulence intensities

Figure 5: DNS of single phase channel flow

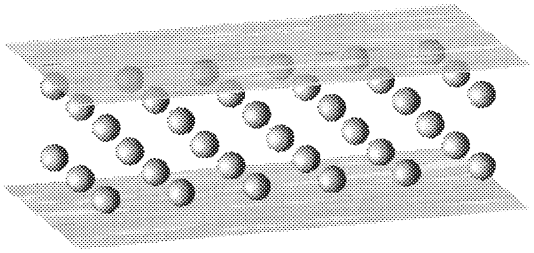

Figure 6: Initial distribution of bubbles at $t^+ = 0$

parameters α, D^+, Fr and We. The influence of the void ratio α for a fixed diameter and surface tension at zero gravitational acceleration is shown in Figure 8(a). The value of C_f is increased as the void ratio α is increased, since the increase in the effective viscosity dominates over the decrease in the density and the modulation of turbulence at low Reynolds numbers. Figure 8(b) shows that C_f is decreased with increasing bubble diameter D^+ for a fixed void ratio $\alpha = 2.9\%$ at zero gravitational acceleration. At this condition, the presence of bubbles enhances the turbulence intensity, and as shown later the increase in the turbulence intensity is larger with smaller bubble diameter because of larger interface area. The influence of the gravitational acceleration in the direction normal to the walls decreases C_f as shown in Figure 8(c) for two diameters at a fixed void ratio $\alpha = 2.9\%$. When the gravitational acceleration is present, bubbles are concentrated toward one wall as shown in Figures 10 and 11. This concentration of bubbles is supposed to suppress turbulent momentum transport in the wall-normal direction. Figure 8(d) shows that effect of the surface tension on C_f is negligible, although the deformation of bubbles is very different as shown in Figure 12.

Figure 9 shows profiles of the turbulence intensity components. The wall-normal and spanwise components are increased by the presence of bubbles, while the peak of the streamwise component is decreased in the high void ratio case. This tendency qualitatively agrees with the measurement by Kato et al. (1999). The increase in the wall-normal and spanwise intensities is larger at $D^+ = 71$ than at $D^+ = 113$ at the same void ratio of $\alpha = 2.9\%$.

The relation between the structure of turbulence and bubbles in the case Run-6 is shown in Figure 13, in which vortex structures are visualized by isosurfaces of the second invariant of the velocity gradient tensor Q, which is defined as

$$Q = \frac{1}{2}\left(W_{ij}W_{ij} - S_{ij}S_{ij}\right) \tag{4}$$

$$W_{ij} = \frac{1}{2}\left(\frac{\partial u_i}{\partial x_j} - \frac{\partial u_j}{\partial x_i}\right) \tag{5}$$

$$S_{ij} = \frac{1}{2}\left(\frac{\partial u_i}{\partial x_j} + \frac{\partial u_j}{\partial x_i}\right) \tag{6}$$

The structure of the wall turbulence is very similar to that without bubbles, suggesting that direct influence of bubbles of this size on

the structure of wall turbulence is weak. Figure 14 shows the average value of Q in the water region versus the distance to the nearest bubble surface. In the region around bubbles the average value of Q takes negative value meaning that bubbles tend to be in high shear region, while the high value of Q at the surface of bubble is due to the vorticity resulting from the curvature and the boundary condition at the surface. This statistics suggest that there is interactions between the vorticity attached to the bubble surface and the structure of turbulence.

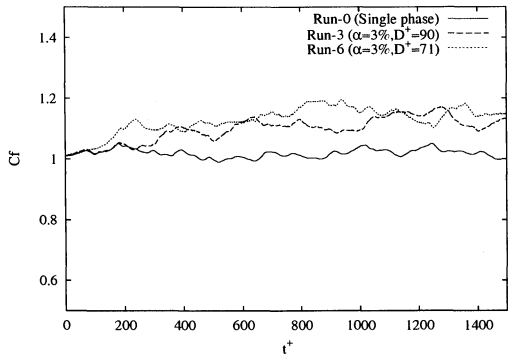

Figure 7: Time history of the normalized friction coefficient

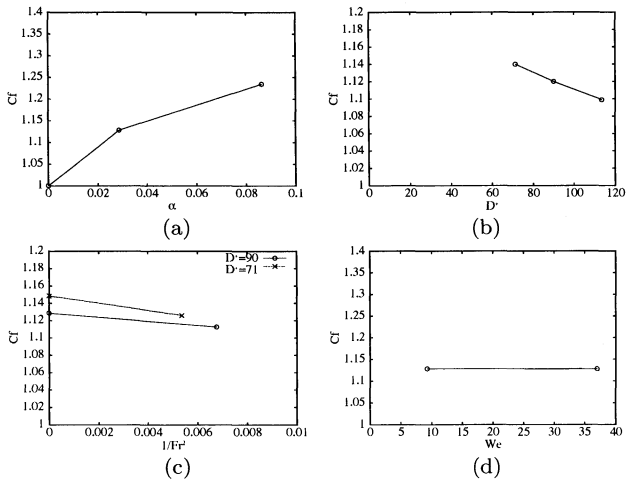

Figure 8: Influence of α, D^+, Fr and We on the friction coefficient

SUMMARY AND CONCLUSIONS

A computational method for investigating the interactions between bubbles and turbulence has been developed in this study. The method employs a special front-tracking method, which tracks individual bubbles by the center positions and radius distributions. The advantage of the new method over front-capturing methods is that the interface curvature can be calculated more accurately for a given grid resolution.

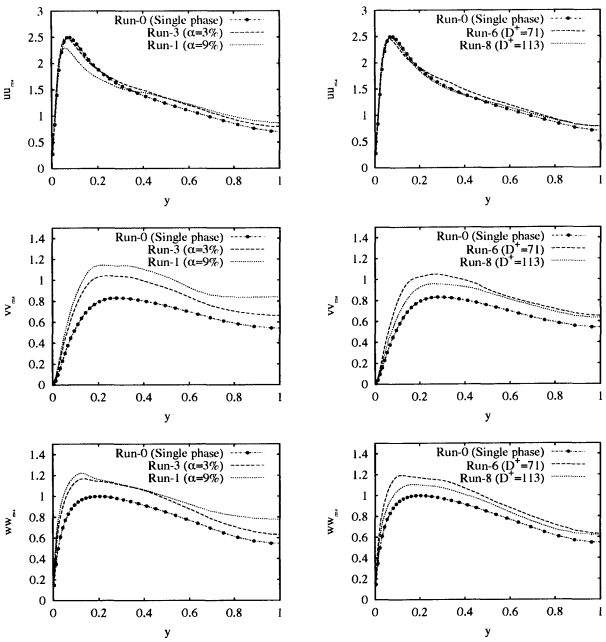

Figure 9: Profiles of turbulence intensities

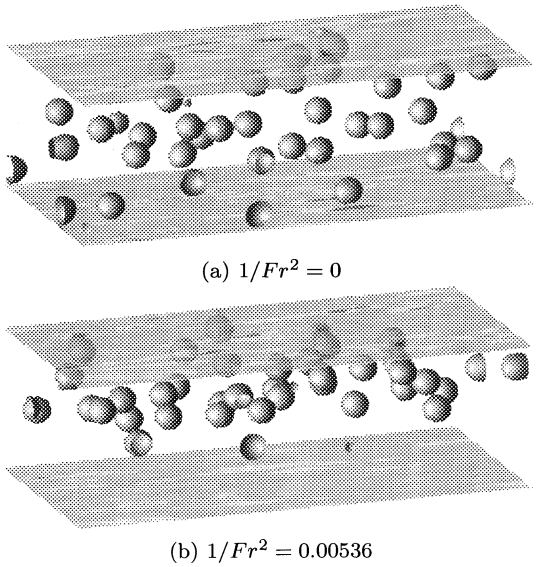

(a) $1/Fr^2 = 0$

(b) $1/Fr^2 = 0.00536$

Figure 10: Distribution of bubbles with or without gravity

This method has been applied to DNS computations of a low Reynolds number turbulent channel flow containing bubbles. The results of DNS show that the turbulence intensity increases and becomes isotropic when bubbles are present. It is also shown that increase in the intensity is lager with smaller bubbles, and that the buoyancy effect is preferable for the drag reduction. These results suggests that large bubbles can be preferable for the drag reduction.

References

Guin, M. M., Kato, H., and Yamaguchi, H., 1996, "Reduction of skin friction by microbub-

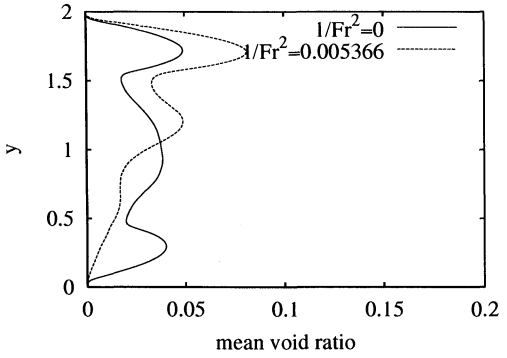

Figure 11: Profiles of the time-averaged void ratio

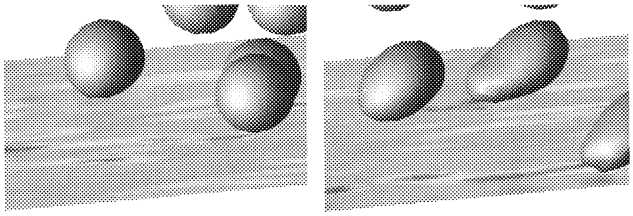

We=9 We=37

Figure 12: Typical shape of bubbles near the wall

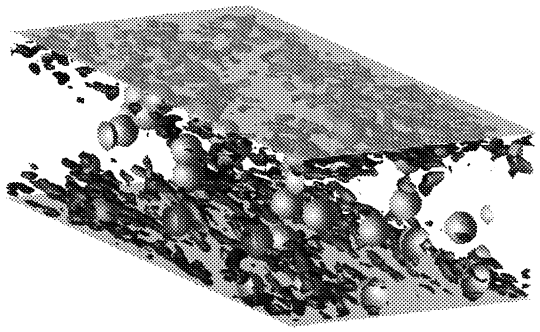

Figure 13: Bubbles and structures of turbulence indicated by isosurfaces of the second invariant of the velocity gradient tensor at a positive value

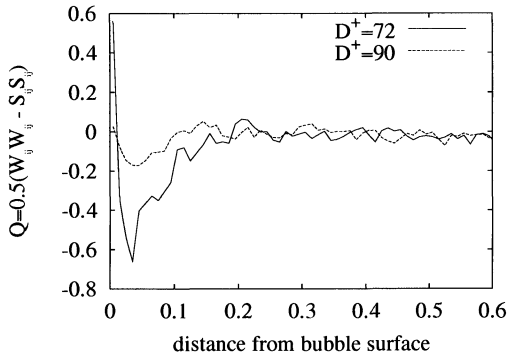

Figure 14: Average value of the second invariant of the velocity gradient tensor versus the distance from the nearest bubble surface

bles and its relation with near-wall bubble concentration in a channel", *Journal of Marine Science and Technology*, Vol. 1, pp. 241–254.

Hirt, C. W., and Nichols, B. D., 1981, "Volume of fluid (VOF) method for the dynamics of free boundaries", *Journal of Computational Physics*, Vol. 39, pp. 201–225.

Kanai, A. and Miyata, H., 1998, "A marker-Density-Function approach for the direct numerical simulations of bubbly flows", *Journal of Society of Naval Architects of Japan*, Vol. 185, pp. 21–30.

Kato, H., Iwashina, T., Miyanaga, M., and Yamaguchi, H., 1999, "Effect of microbubbles on the structure of turbulence in a turbulent boundary layer", *Journal of Marine Science and Technology*, Vol. 4, pp. 155–162.

Kim, J., Moin, P., and Moser, R., 1986, "Turbulence statistics in fully developed channel flow at low Reynolds number", *Journal of Fluid Mechanics*, Vol. 177, pp. 133–166.

Madavan, N. K., Deutsch, S., and Merkle, C. L. , "Measurements of local skin friction in a microbubble-modified turbulent boundary layer", 1985, *Journal of Fluid Mechanics*, Vol. 156, pp. 237–256.

McCormick, M. E. and Bhattacharyya, R., 1973, "Drag reduction of a submersible hull by electrolysis", *Naval Engineers Journal*, Vol. 85, pp. 11–16.

Takahashi, T., Kakugawa, A., and Kodama, Y., 1997, "Streamwise distribution of the skin friction reduction by microbubbles", *Journal of Society of Naval Architects of Japan*, Vol. 182, pp. 1–8.

Tominaya, A., Kataoka, I., and Sakaguchi, T., 1995, "Drag Coefficients of Bubbles (1st Report, Drag Coefficients of a Single Bubble in a Stagnant Liquid)", *Journal of the Japan Society of Mechanical Engineers B*, Vol. 61(587), pp. 2357–2364.

Unverdi, S. O., and Tryggvason, G., 1992, "A Front-Tracking Method for Viscous, Incompressible, Multi-fluid Flows", *Journal of Computational Physics*, Vol. 100, pp. 25–37.